J. Biochem 2023;174(1):59–69 https://doi.org/10.1093/jb/mvad019

JB THE JOURNAL OF BIOCHEMISTRY

# Biochemical characterization of the RNA-binding and RNA–DNA strand exchange activities of the human RAD52 protein

*Received 14 December 2022; accepted 17 February 2023; published online 22 February 2023*

**Ryohei Tsuchiya, Mika Saotome, Chiaki Kinoshita, Kazuki Kamoi and Wataru Kagawa†**

Department of Chemistry, Graduate School of Science and Engineering, Meisei University, 2-1-1 Hodokubo, Hino-shi, Tokyo 191-8506, Japan
†Wataru Kagawa, Department of Chemistry, Graduate School of Science and Engineering, Meisei University, 2-1-1 Hodokubo, Hino-shi, Tokyo 191-8506, Japan. Tel.: +81-42-591-5595, Fax: +81-42-591-7419, email: wataru.kagawa@meisei-u.ac.jp

**RAD52 is a single-stranded DNA (ssDNA) binding protein that functions in the repair of DNA double-strand breaks (DSBs) by promoting the annealing of complementary DNA strands. RAD52 may also play an important role in an RNA transcript-dependent type of DSB repair, in which it reportedly binds to RNA and mediates the RNA–DNA strand exchange reaction. However, the mechanistic details of these functions are still unclear. In the present study, we utilized the domain fragments of RAD52 to biochemically characterize the single-stranded RNA (ssRNA) binding and RNA–DNA strand exchange activities of RAD52. We found that the N-terminal half of RAD52 is primarily responsible for both activities. By contrast, significant differences were observed for the roles of the C-terminal half in RNA–DNA and DNA–DNA strand exchange reactions. The C-terminal fragment stimulated the inverse RNA–DNA strand exchange activity displayed by the N-terminal fragment in *trans*, whereas the *trans* stimulatory effect by the C-terminal fragment was not observed in the inverse DNA–DNA or forward RNA–DNA strand exchange reactions. These results suggest the specific function of the C-terminal half of RAD52 in RNA-templated DSB repair.**

*Keywords:* RNA; protein-nucleic acid interaction; intrinsically disordered region; homologous recombination; DNA repair.

**Graphical Abstract**

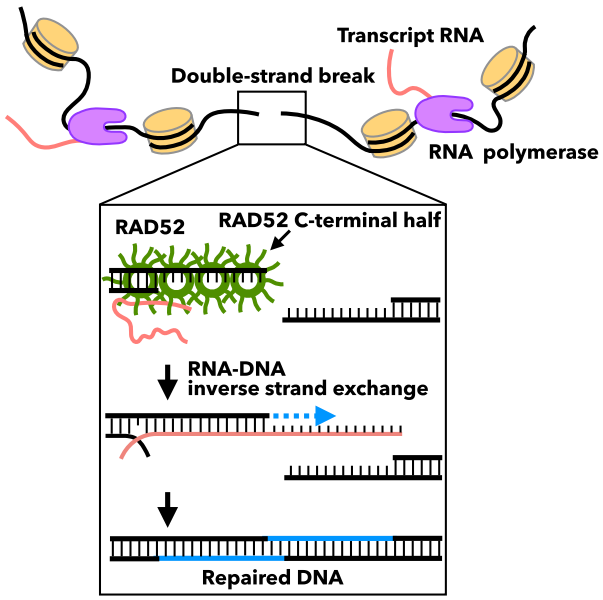


## Introduction

Homologous recombination (HR) is one of the fundamental mechanisms for repairing DNA double-strand breaks (DSBs). Defects in HR can lead to genomic instability by causing mutations in the genome or gross chromosomal rearrangements, such as deletions, insertions and loss of heterozygosity *(1, 2)*. Failure to repair such DNA damages may eventually lead to cancer *(3, 4)*. The high fidelity of HR is made possible by the use of the undamaged sister chromatid as the template for DNA synthesis during repair. In eukaryotes, the RAD51 protein is a critical component of HR. It promotes the base pair formation between the single-stranded region of the damaged DNA, and the homologous duplex region of the template DNA at the proper location, in a reaction called DNA strand exchange (hereafter referred to as DNA–DNA strand exchange). It is a crucial step for error-free DSB repair *(5)*.

Several lines of evidence suggest that HR is involved in the repair of DSBs occurring at transcriptionally active regions of the genome *(6, 7)*. At these regions, large amounts of the transcribed RNA are presumed to be located nearby or associated with the transcribed DNA region via base pairing to form an R-loop structure. Previous studies have revealed two potential roles for RNA in HR. One is the recruitment of DNA repair factors to the DSB, in which R-loops act as a signal for initiating HR. The repair factors RAD52, BRCA1 and XPG are reportedly recruited to R-loops formed at transcriptionally active genomic regions to initiate HR in human cells *(8)*. The other potential role of RNA transcripts is to directly serve as templates for HR. In *Saccharomyces cerevisiae*, RNA-templated repair reportedly occurs in the absence of ribonuclease and is dependent on *RAD52 (9)*. RNA-templated repair may also occur in human cells in the G0/G1 phase, in a RAD52-dependent mechanism *(10, 11)*.

*In vitro*, the yeast and human RAD52 proteins efficiently promoted the strand exchange reaction between

single-stranded RNA (ssRNA) and its homologous double-stranded DNA (dsDNA), when RAD52 was first incubated with dsDNA, followed by the addition of ssRNA, in a reaction described as 'inverse' strand exchange *(12)*. The 'inverse' reaction was originally proposed for the bacterial RecA recombinase-mediated strand exchange between single-stranded DNA (ssDNA) and dsDNA, in which RecA first forms a complex with dsDNA and then associates with ssDNA *(13, 14)*. This reaction is distinct from the canonical strand exchange, in which the recombinase first forms a complex with ssDNA (or ssRNA), which then searches for sequence homology in the dsDNA, in a reaction referred to as 'forward' strand exchange. Notably, Rad52 also reportedly promoted the forward strand exchange between ssRNA (or ssDNA) and dsDNA, but with lower efficiency *(9, 12)*. The human RAD52 protein also facilitated the ligation of DSB ends by hybridizing the two DSB ends to a homologous RNA transcript *(15)*. These are potential mechanisms for RNA-templated repair and suggest that RAD52 may have important functions with RNA. However, RAD52 is also an ssDNA binding protein and stimulates the annealing reaction between complementary DNA strands *(16–18)*. This activity is important for the single-strand annealing pathway in homology-directed repair *(18–20)*. At the molecular level, it is unclear how RAD52 can accommodate both types of nucleic acids and exhibit a multitude of activities during DSB repair.

The role of the N-terminal half of RAD52 in HR has been extensively studied. In yeast, the C-terminally truncated *rad52* mutants retained partial DSB repair activity, suggesting that the core activity of *RAD52* is associated with the N-terminal half of the protein *(21)*. Biochemical studies revealed that the isolated N-terminal half is capable of promoting DNA annealing, D-loop formation and inverse RNA–DNA strand exchange reactions *(22–24)*. Structural studies have shown that the full-length RAD52 protein oligomerizes into a ring structure *(25–27)*. The atomic resolution structures of the isolated N-terminal half *(28, 29)* facilitated detailed studies that identified the key amino acid residues for DNA binding *(22, 30, 31)*. These studies, along with the single-molecule studies of RAD52 *(32, 33)*, have provided crucial insights into the underlying mechanisms of RAD52-mediated DNA annealing.

In contrast, very little information on the functions and mechanisms of the C-terminal half of RAD52 is available. Most of the C-terminal region is predicted to be intrinsically disordered *(34, 35)*, and it contains regions for RPA and RAD51 binding *(36–39)*. In yeast Rad52, these binding sites are important for loading the Rad51 recombinase onto RPA-coated DSB sites *(40, 41)*. In addition, a second DNA binding site is present in the C-terminal one-third of the protein and binds to both ssDNA and dsDNA *(42)*. Truncation of the C-terminal region in yeast Rad52 impairs its ability to stimulate Rad51-mediated DNA–DNA strand exchange *(38)*. Thus, the mediator function of yeast Rad52 is dependent on the C-terminal half. However, besides this mediator activity, the function of the C-terminal half remains enigmatic.

In the present study, we biochemically characterized the ssRNA binding activity of human RAD52, by comparisons with its ssDNA binding activity. RAD52 exhibited similar affinities towards ssRNA and ssDNA, suggesting that it also plays an important role in RNA metabolism. The N-terminal half of RAD52 was primarily responsible for the affinities for ssRNA and ssDNA, and mediating forward and inverse RNA–DNA strand exchange, as well as inverse DNA–DNA strand exchange reactions. Conversely, we observed the specific role of the C-terminal half in the inverse RNA–DNA strand exchange reaction, but not in the inverse DNA–DNA or forward RNA–DNA strand exchange reactions.

## Materials and Methods

### *Proteins*

The full-length RAD52 protein (Uniprot ID: P43351) and its N-terminal fragment containing amino acid residues 1 to 212 ($RAD52^{1–212}$) were purified as described *(22)*, using Ni-NTA agarose and SP Sepharose column chromatography. The C-terminal fragment of RAD52, containing amino acid residues 184 to 418, was prepared by initially expressing an N-terminally hexahistidine-tagged full-length construct with a TEV protease recognition amino acid sequence inserted between the RAD52 amino acid residues Pro183 and Leu184. This construct was expressed in the *Escherichia coli* JM109(DE3) strain. Typically, the *E. coli* were cultured in 1.6-L LB medium at 30°C. When the culture reached an optical density ($A_{600}$) of 0.6, protein expression was induced with 0.5 mM IPTG, and the culture was continued overnight. The following day, the cells were collected by centrifugation and resuspended in buffer A (50 mM Tris–HCl, pH 7.8, 0.3 M KCl, 10% glycerol, 5 mM 2-mercaptoethanol) containing 10 mM imidazole. The resuspended cells were disrupted by sonication, and centrifuged at 32,300*g* for 30 min to remove insoluble material. The supernatant was batch-mixed with 2 mL of Ni-NTA agarose at 4°C on a rotator for 15 min. The protein-bound agarose beads were batch-washed with buffer A containing 50 mM imidazole (50 mL x 2). After the washed agarose beads were resuspended in 2 mL of buffer A containing 50 mM imidazole, approximately 1 mg of TEV protease was added to the mixture, which was gently mixed on a rotator at 4°C for 1 h. The beads were then centrifuged, and the supernatant, which contained the C-terminal fragment ($RAD52^{184–418}$), was concentrated with a Vivaspin Turbo 4 centrifugal filter (10K MWCO) to a volume of approximately 1 mL. The concentrated fraction was purified on either an ENrich SEC 650 column (Bio-Rad) or a Superdex 200 Increase column (Cytiva) pre-equilibrated with buffer B (50 mM Tris–HCl, pH 7.8, 0.3 M KCl, 2 mM 2-mercaptoethanol and 5% glycerol). Peak fractions were collected, concentrated to approximately 2 mg/mL with a Vivaspin Turbo 4 centrifugal filter (10K MWCO), and stored at −80°C. The concentration of $RAD52^{184–418}$ was determined from the absorbance at 280 nm by using an extinction coefficient of 20,970 $M^{-1}$ $cm^{-1}$, which was calculated with the Protparam tool on the ExPASy website (https://web.expasy.org/protparam/).

### *DNA and RNA substrates*

All DNA and RNA substrates were purchased from FASMAC Co., Ltd. (Kanagawa, Japan) and Hokkaido System Science Co., Ltd. (Hokkaido, Japan). The HPLC-purified

oligonucleotides were as follows: ISE#1 (40-mer Cy3-labeled ssDNA, 5′-ACA GCA CCA GAT TCA GCA ATT AAG CTC TAA GCC ATC CGC A-3′), ISE#2 (71-mer ssDNA, 5′-TGC GGA TGG CTT AGA GCT TAA TTG CTG AAT CTG GTG CTG TAG GTC AAC ATG TTG TAA ATA TGC AGC TAA AG-3′), ISE#3 (40-mer Cy5-labeled ssRNA, 5′-UGC GGA UGG CUU AGA GCU UAA UUG CUG AAU CUG GUG CUG U-3′), ISE#4 (40-mer Cy5-labeled ssDNA, 5′-TGC GGA TGG CTT AGA GCT TAA TTG CTG AAT CTG GTG CTG T-3′) and CA#1 (40-mer Cy5-labeled ssRNA, 5′- AAU ACC GCA UCA GGA AAU UGU AAG CGU UAA UAU UUU GUU A-3′). In addition, for the competitive binding assay, the following reverse phase-purified oligonucleotides were used: CA#2 (40-mer ssDNA, 5′-ACA GCA CCA GAT TCA GCA ATT AAG CTC TAA GCC ATC CGC A-3′) and CA#3 (40-mer ssRNA, 5′-AAU ACC GCA UCA GGA AAU UGU AAG CGU UAA UAU UUU GUU A-3′). All oligonucleotides were dissolved in TE (10 mM Tris–HCl, pH 8.0, 1 mM EDTA) and stored at −30°C. To prepare the dsDNA substrate used in the strand-exchange assays, ISE#1 and ISE#2 were annealed in a 40-$\mu$L solution, containing 30 mM Hepes-KOH, pH 7.5, 0.1 M NaCl, 5 mM $MgCl_2$ and 0.1 mM 2-mercaptoethanol. The final concentrations of ISE#1 and ISE#2 were 625 and 938 nM, respectively. The mixture was placed in a thermal cycler, heated for 2 min at 92°C and then incubated for 10 min at 34°C. The mixture was fractionated through a 12% polyacrylamide gel, and the DNA was visualized by SYBR Gold staining. The band corresponding to the annealed product was excised and purified by a crush-and-soak method, essentially as described *(43)*. All RNA and DNA concentrations are expressed in moles of molecules.

#### *Electrophoretic mobility shift assays*

The indicated concentrations of RAD52 and nucleic acids (described in detail in the figure legends) were mixed in a reaction mixture (20 $\mu$L), containing 20 mM Hepes-NaOH, pH 7.5, 2 mM 2-mercaptoethanol and 0.01 mg/mL bovine serum albumin (New England Biolabs). In the reaction mixtures containing ssRNA, 0.25 U/$\mu$L RNase inhibitor (New England Biolabs) was included. The reaction mixture was incubated at 37°C for 10 min, and then 4 $\mu$L of 40% sucrose was added. The mixture was fractionated through a 2% agarose gel at 2.9 V/cm for 120 min using a submarine gel electrophoresis system (NIHON EIDO) or a 12% polyacrylamide gel at 75 V for 90 min using a Mini-PROTEAN Tetra Cell apparatus (Bio-Rad). The gels were visualized with an FLA7000 Typhoon Image Analyzer.

For the assay using an ssDNA competitor, a 16-$\mu$L reaction mixture, containing 2 $\mu$L of Cy5-labeled 625 nM ssRNA (CA#1), 4 $\mu$L of EMSA Buffer (0.1 M Hepes-NaOH, pH 7.5, 10 mM 2-mercaptoethanol), 1 $\mu$L of 0.2 mg/mL bovine serum albumin (New England Biolabs), 1 $\mu$L of 5 U/$\mu$L RNase inhibitor (New England Biolabs) and 8 $\mu$L of $H_2O$ was incubated at 37°C for 5 min. Afterwards, 2 $\mu$L of 10 $\mu$M RAD52 was added and incubated for 10 min. Aliquots (2 $\mu$L) of the indicated concentrations of ssDNA competitor (CA#2) were added, and the reaction was continued for 10 min. Prior to electrophoresis, 4 $\mu$L of 40% sucrose was added to the reaction mixture. The mixture was fractionated through a 2% agarose gel at 2.9 V/cm for 120 min. The gels were visualized with an FLA 7000 Typhoon Image Analyzer.

The assay using an ssRNA competitor was performed as described above, with the exceptions of substituting the Cy5-labeled ssRNA (CA#1) with Cy3-labeled ssDNA (ISE#1) and the ssDNA competitor (CA#2) with an ssRNA competitor (CA#3).

#### *Inverse strand exchange assay*

Inverse RNA–DNA and DNA–DNA strand exchange assays were performed essentially as described *(12)*, with some modifications. For the inverse RNA–DNA strand exchange reaction, a 16-$\mu$L reaction mixture, containing 2 $\mu$L of Cy3-labeled 676 nM dsDNA (prepared from ISE#1 and ISE#2), 4 $\mu$L of Strand Exchange Buffer (0.1 M Hepes-KOH, pH 7.5, 25 mM $MgCl_2$, 10 mM 2-mercaptoethanol), 1 $\mu$L of 0.2 mg/mL bovine serum albumin (New England Biolabs), 1 $\mu$L of 5 U/$\mu$L RNase inhibitor (New England Biolabs) and 8 $\mu$L of $H_2O$ was incubated at 37°C for 5 min. Afterwards, 2 $\mu$L of 10 $\mu$M RAD52 was added and incubated for 10 min. The strand exchange reaction was initiated by adding 2 $\mu$L of 2.5 $\mu$M Cy5-labeled ssRNA (ISE#3). After incubations for the indicated times at 37°C, the substrates and products were deproteinized by adding 2 $\mu$L of 5% LDS (lithium dodecyl sulfate) and 1 $\mu$L of proteinase K (800 U/mL, New England Biolabs), followed by a 10 min incubation at 37°C. Prior to electrophoresis, 4 $\mu$L of 40% sucrose was added. The mixture was then fractionated through a 12% polyacrylamide gel at 75 V for 90 min, using a Mini-PROTEAN Tetra Cell apparatus (Bio-Rad). The gel was scanned for Cy3 and Cy5 fluorescence with an FLA 7000 Typhoon Image Analyzer. The percentages of products were calculated by quantifying the Cy3 signals from the dsDNA substrate and the strand exchange product, using the Fiji software *(44)*.

The inverse DNA–DNA strand exchange reaction was performed as described above, with the exceptions of substituting ssRNA (ISE#3) for ssDNA (ISE#4) and excluding the RNase inhibitor.

#### *Forward strand exchange assay*

For the forward RNA–DNA strand exchange reaction, a 16-$\mu$L reaction mixture, containing 2 $\mu$L of 2.5 $\mu$M Cy5-labeled ssRNA (ISE#3), 4 $\mu$L of Strand Exchange Buffer (0.1 M Hepes-KOH, pH 7.5, 25 mM $MgCl_2$, 10 mM 2-mercaptoethanol), 1 $\mu$L of 0.2 mg/mL bovine serum albumin (New England Biolabs), 1 $\mu$L of 5 U/$\mu$L RNase inhibitor (New England Biolabs) and 8 $\mu$L of $H_2O$ was incubated at 37°C for 5 min. Afterwards, 2 $\mu$L of 10 $\mu$M RAD52 was added and incubated for 10 min. The strand exchange reaction was initiated by adding 2 $\mu$L of Cy3-labeled 676 nM dsDNA (prepared from ISE#1 and ISE#2). After incubations for the indicated times at 37°C, the substrates and products were deproteinized by adding 2 $\mu$L of 5% LDS (lithium dodecyl sulfate) and 1 $\mu$L of proteinase K (800 U/mL, New England Biolabs), followed by a 10 min incubation at 37°C. Prior to electrophoresis, 4 $\mu$L of 40% sucrose was added. The mixture was then fractionated through a 12% polyacrylamide gel at 75 V for 90 min, using a Mini-PROTEAN Tetra Cell apparatus (Bio-Rad). The gel was scanned for Cy3 and Cy5 fluorescence with

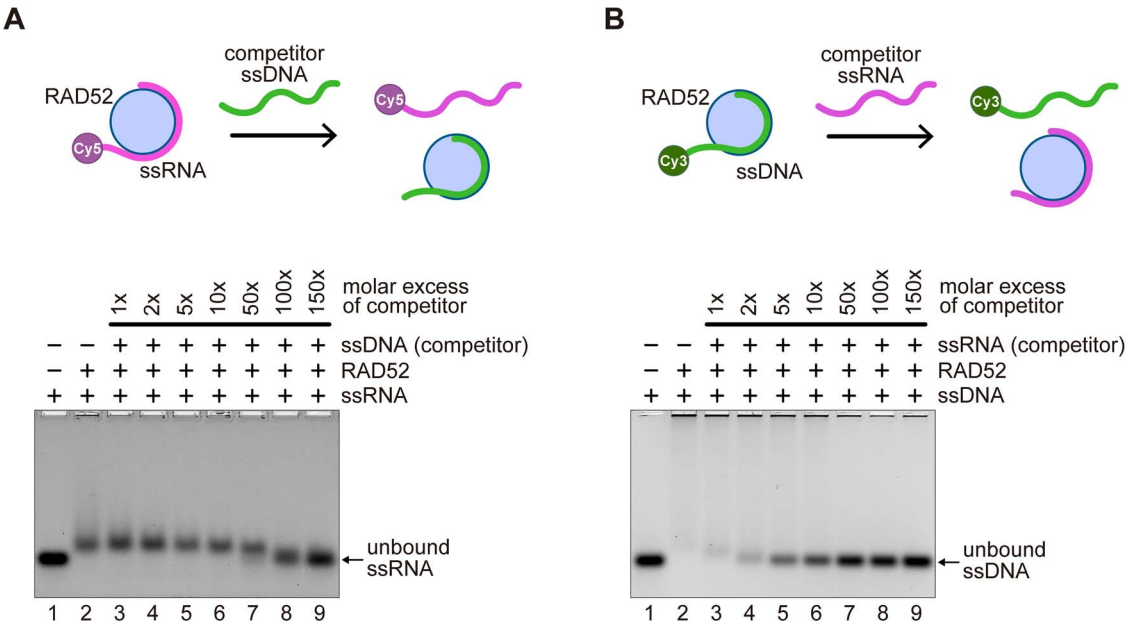


**Fig. 2. ssRNA- and ssDNA-binding affinities of RAD52 compared by a competitive assay.** Schematic diagrams of the competitive assays are shown at the top. (**A**) RAD52 binding to ssRNA was competed with excess amounts of ssDNA. RAD52 (1 $\mu$M) was incubated with ssRNA (CA#1, 62.5 nM) for 10 min at 37°C, and then the competitor ssDNA (CA#2) was added at 1× (62.5 nM), 2× (125 nM), 5× (312.5 nM), 10× (625 nM), 50× (3125 nM), 100× (6250 nM) and 150× (9375 nM) molar excesses. (**B**) RAD52 binding to ssDNA was competed with excess amounts of ssRNA. RAD52 (1 $\mu$M) was incubated with ssDNA (ISE#1, 62.5 nM) for 10 min at 37°C, and then the competitor ssRNA (CA#3) was added at 1× (62.5 nM), 2× (125 nM), 5× (312.5 nM), 10× (625 nM), 50× (3125 nM), 100× (6250 nM) and 150× (9375 nM) molar excesses. The assay was repeated three times independently, and similar results were obtained.

an FLA 7000 Typhoon Image Analyzer. The percentages of products were calculated by quantifying the Cy3 signals from the dsDNA substrate and the strand exchange product, using the Fiji software.

## Results

### *RAD52 binds to ssRNA with an affinity comparable to that of ssDNA*

To compare the ssRNA and ssDNA binding activities of RAD52, RAD52 was added to a reaction mixture containing both ssRNA and ssDNA, which were 5′-end labeled with Cyanine 5 (Cy5) and Cyanine 3 (Cy3) fluorescent dyes, respectively (Fig. 1A). The sequences of the two nucleic acid substrates were designed so that they do not hybridize with each other. The reaction mixtures were resolved through an agarose gel, and Cy5 and Cy3 fluorescence signals were detected to visualize both complexes. To accurately quantify the percentage of complexes formed, a portion of the reaction mixture was also separated through a polyacrylamide gel, which allowed enhanced resolution of the unbound substrates and the complexes. The quantification results are shown in Fig. 1C. At increased RAD52 concentrations, the simultaneous shifting of both ssRNA and ssDNA was observed (Fig. 1B, lanes 4–6 and 1C). These results indicated that RAD52 has similar affinities for ssRNA and ssDNA. A closer inspection of the complexes revealed that most of the RAD52–ssRNA complexes entered the gel and had a smeared appearance, whereas the RAD52–ssDNA complex mostly remained in the gel well. These differences suggest that RAD52 may more readily form large complexes when bound to ssDNA, as compared to RAD52 bound to ssRNA.

To further characterize the ssRNA binding activity of RAD52, we examined the ssRNA binding in the presence of competitors. The initial RAD52–ssRNA complex was formed at a RAD52 concentration in which no unbound ssRNA was observed (Fig. 2A, lane 2). To this complex, various amounts of competitor ssDNA (up to 150-fold molar excess) were added, and the reaction mixtures were fractionated through an agarose gel. The unbound ssRNA was clearly observed in the presence of a 100-fold molar excess of the competitor ssDNA (Fig. 2A, lane 8). By contrast, when the ssDNA binding was examined in the presence of the competitor ssRNA, the unbound ssDNA was observed in the presence of a 5-fold molar excess of the competitor ssRNA (Fig. 2B, lane 5). These results suggest that the RAD52–ssRNA nucleoprotein complex is more stable than the RAD52–ssDNA nucleoprotein complex.

### *The N-terminal and C-terminal halves of RAD52 contain ssRNA binding regions*

To gain more insights into the interactions between RAD52 and ssRNA, the ssRNA and ssDNA binding activities of the full-length, N-terminal and C-terminal fragments of RAD52 (Fig. 3, A and B) were examined by electrophoretic mobility shift assays (EMSA). Complexes were visualized by resolving the reaction mixture through an agarose gel. In the presence of 1 $\mu$M RAD52, most of the substrates were shifted (Fig. 3C, lanes 3 and 8). Since the full-length RAD52 protein oligomerizes into an 11-mer ring *(27)*, this concentration is equivalent to approximately 90 nM of oligomeric rings. Thus, our results suggest that the full-length RAD52 protein efficiently binds to both ssRNA and ssDNA, because complete binding of the substrates was observed at nearly equimolar amounts

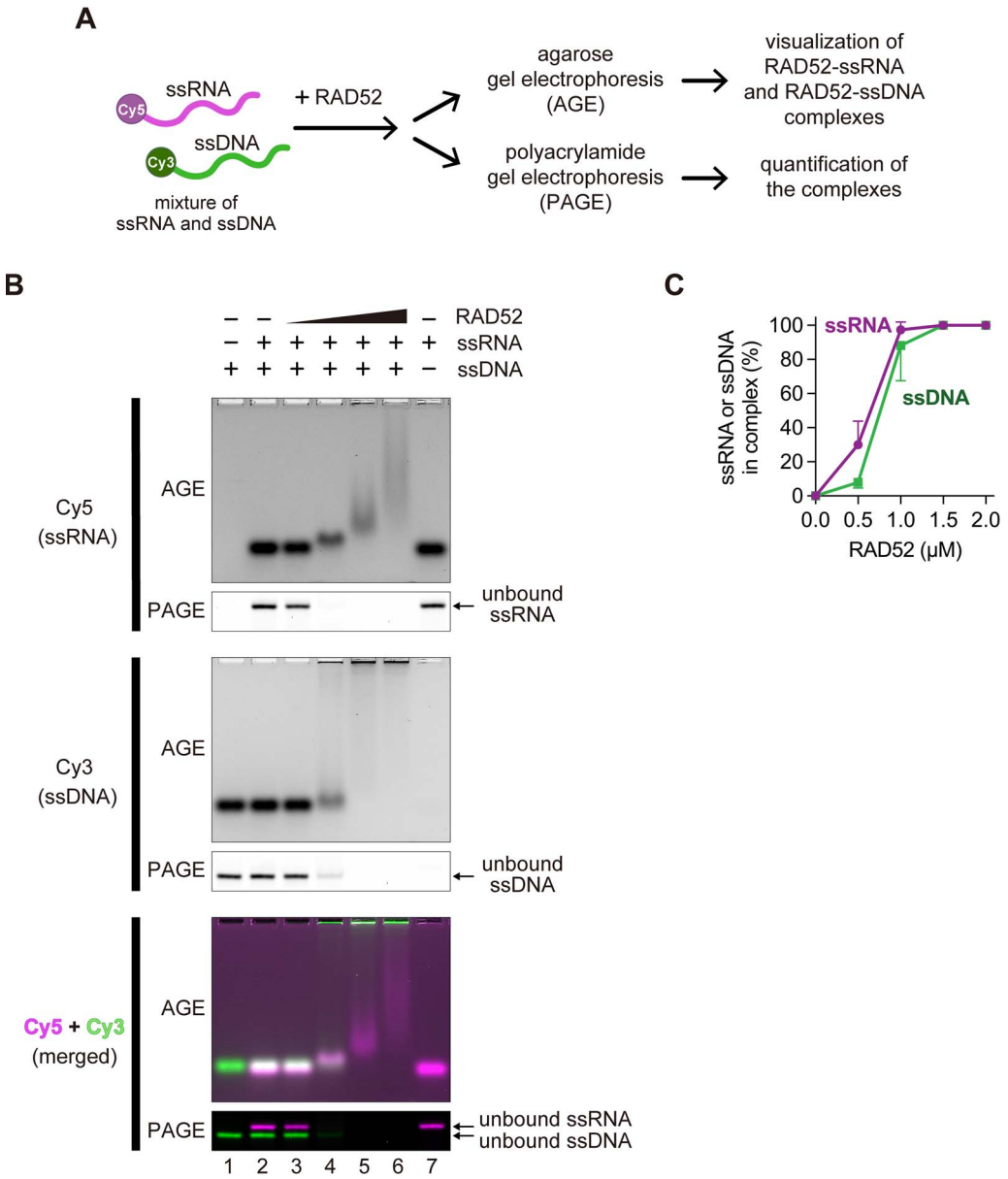


**Fig. 1. ssRNA-binding activity of RAD52.** (**A**) A schematic diagram of the ssRNA binding assay. Equimolar concentrations of ssRNA and ssDNA were mixed with RAD52, and the resulting RAD52–ssRNA and RAD52–ssDNA complexes were resolved by agarose and polyacrylamide gel electrophoresis. The complexes were detected by the fluorescence from the Cy5 and Cy3 dyes attached to the nucleic acids. (**B**) A representative result from three independent experiments is shown. RAD52 (0.5, 1, 1.5 or 2 $\mu$M) was incubated with ssRNA (CA#1, 62.5 nM) and ssDNA (ISE#1, 62.5 nM) for 10 min at 37°C, and the complexes were fractionated through agarose and polyacrylamide gels (indicated as AGE and PAGE, respectively). Cy5 and Cy3 signals from the same agarose and polyacrylamide gels are shown. For the polyacrylamide gel, only the unbound substrate is shown. The bottom gel images are an overlap of the Cy5 (top) and Cy3 (middle) images, where Cy5 is colored magenta and Cy3 is colored green. An overlap of Cy5 and Cy3 results in a white color. (**C**) Percentages of complexes formed by RAD52. The percentages were calculated by quantifying the fraction of unbound nucleic acids, using the Fiji software. The data show an average of three independent experiments. The error bars represent the standard deviation.

of the RAD52 oligomeric ring (90 nM) and the nucleic acid substrates (62.5 nM).

The N-terminal fragment (RAD52-N) showed lower affinities for ssRNA and ssDNA, as compared with those of the full-length protein (Fig. 3D). At higher protein concentrations, however, RAD52-N formed large complexes that remained in the gel wells, much like the complexes formed by the full-length protein. The C-terminal fragment (RAD52-C) also bound to ssRNA and ssDNA (Fig. 3E), but with much lower affinities as compared to those of RAD52-N. The complexes did not appear as discrete bands and had a smeared appearance near the unbound substrate. These results suggest that ssRNA binding regions are present in both the N-terminal and C-terminal halves of RAD52.

### *The C-terminal half of RAD52 plays a stimulatory role in inverse RNA–DNA strand exchange*

Previously, RAD52 was shown to promote the inverse strand exchange between dsDNA and its homologous ssRNA, in a reaction where RAD52 is initially mixed with

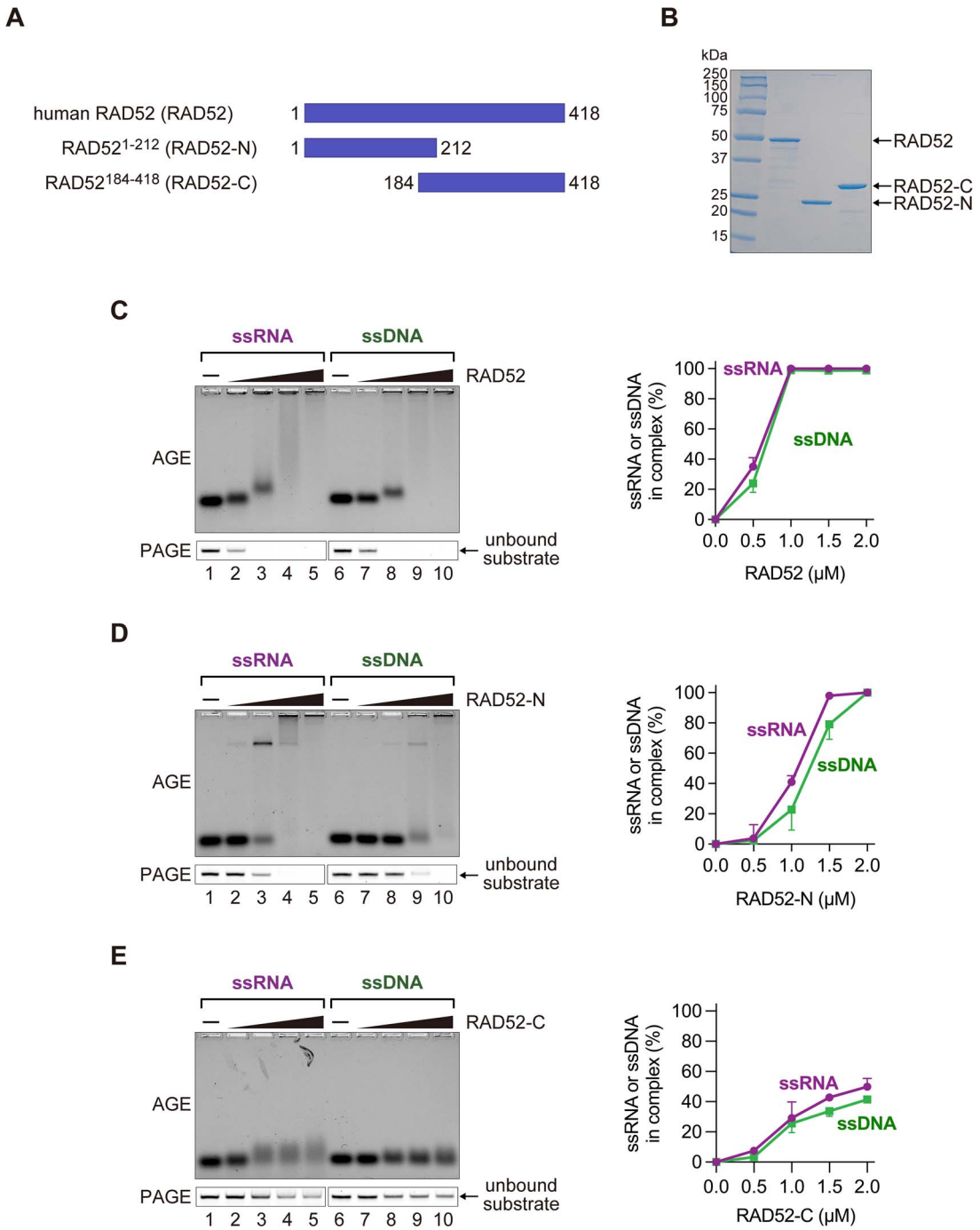


**Fig. 3. ssRNA- and ssDNA-binding activities of the isolated N- and C-terminal domains of RAD52.** (**A**) A schematic diagram of the primary structures of the isolated N- and C-terminal domains of RAD52 used in this study. (**B**) SDS-PAGE of the purified full-length RAD52, RAD52-N and RAD52-C proteins. One $\mu$g of each purified protein was fractionated through a 10–20% gradient gel. ssRNA- and ssDNA-binding activities of the full-length RAD52 protein (**C**), RAD52-N (**D**) and RAD52-C (**E**). Proteins (0.5, 1, 1.5 or 2 $\mu$M) were incubated with ssRNA (ISE#3, 62.5 nM) or ssDNA (ISE#4, 62.5 nM) for 10 min at 37°C and resolved by agarose and polyacrylamide gel electrophoresis (indicated as AGE and PAGE, respectively). The complexes were detected by the fluorescence from the Cy5 dye attached to the nucleic acids. For the polyacrylamide gel, only the unbound substrate is shown. Percentages of complexes formed by RAD52 were calculated by quantifying the fraction of unbound nucleic acids, using the Fiji software. The graph shows an average of three independent experiments. The error bars represent the standard deviation.

dsDNA, and then the ssRNA is added *(12)*. To examine the inverse RNA–DNA strand exchange activities of RAD52-N and RAD52-C, we used Cy5- and Cy3-labeled oligonucleotides as substrates in the reactions (Fig. 4A). Consistent with previous reports, the full-length RAD52 protein converted more than one-third of the dsDNA substrate into RNA–DNA hybrids (Fig. 4B and C). The inverse RNA–DNA strand exchange activity of RAD52-N was partially defective and approximately one-half of that of the full-length protein (Fig. 4C and Supplementary Fig. S1). In contrast, the inverse RNA–DNA strand exchange activity of RAD52-C was barely detectable (Fig. 4C and

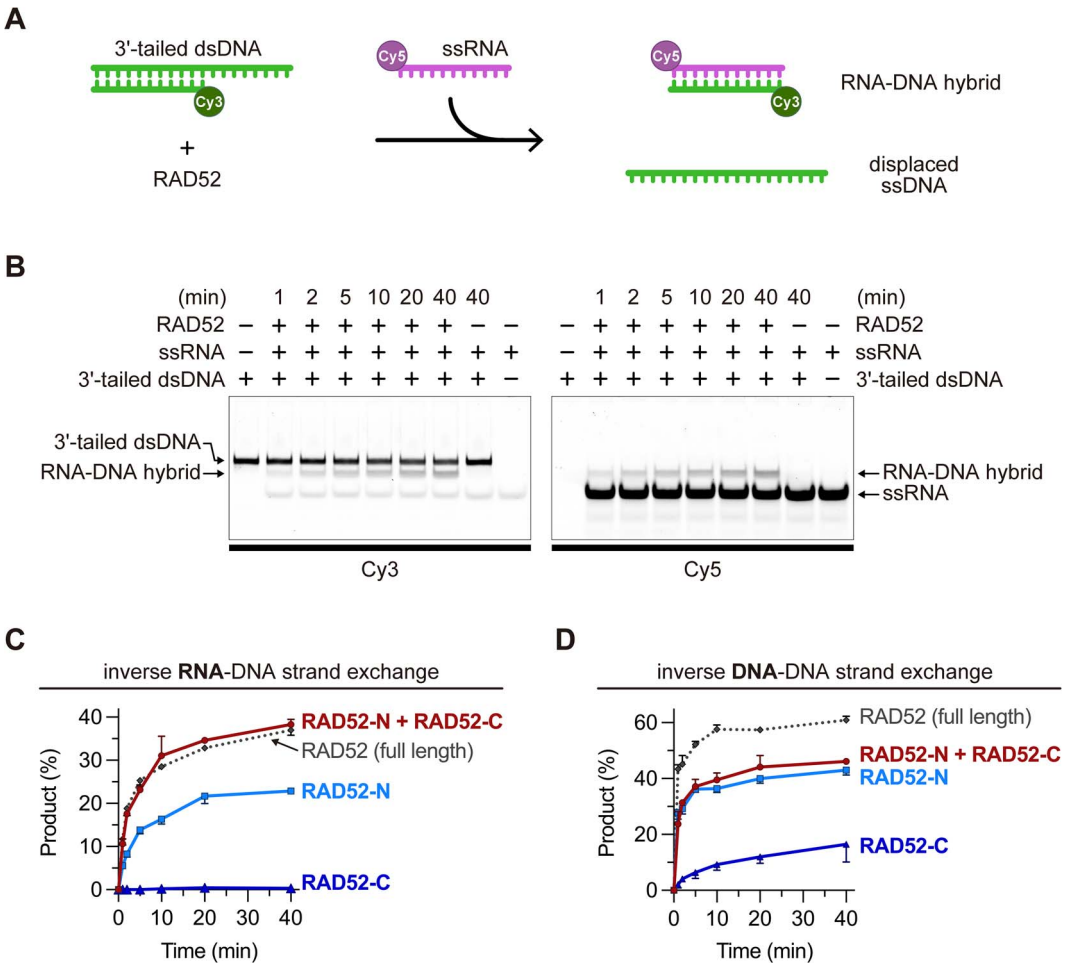


**Fig. 4. Inverse RNA–DNA and DNA–DNA strand exchange activities of the isolated N- and C-terminal domains of RAD52.** (**A**) A schematic diagram of the inverse RNA–DNA strand exchange reaction promoted by RAD52. (**B**) A representative result of the inverse RNA–DNA strand exchange promoted by the full-length RAD52 protein. The left and right gel images are taken from the same gel. RAD52 (1 $\mu$M) was first incubated with dsDNA (ISE#1/ISE#2, 67.6 nM) for 10 min at 37°C, followed by the addition of ssRNA (ISE#3, 250 nM) to initiate the strand exchange reaction. The reaction mixture was incubated at 37°C for the indicated times. Prior to fractionation by PAGE, the substrates and products were deproteinized with proteinase K and LDS (lithium dodecyl sulfate). (**C**) Percentages of inverse RNA–DNA strand exchange catalysed by RAD52-N (1 $\mu$M), RAD52-C (1 $\mu$M) and both RAD52-N (1 $\mu$M) and RAD52-C (1 $\mu$M), plotted as a function of time. (**D**) Percentages of inverse DNA–DNA strand exchange catalysed by the full-length RAD52 protein (1 $\mu$M), RAD52-N (1 $\mu$M), RAD52-C (1 $\mu$M) and both RAD52-N (1 $\mu$M) and RAD52-C (1 $\mu$M), plotted as a function of time. All assays were repeated three times independently. Graphs show averages of three independent experiments. The error bars represent the standard deviation.

Supplementary Fig. S1). These results indicate that the catalytic site for inverse RNA–DNA strand exchange is located in the N-terminal half of RAD52.

Interestingly, when RAD52-C was added together with RAD52-N in the strand exchange reaction, the strand exchange activity was nearly equivalent to that of the full-length protein (Fig. 4C and Supplementary Fig. S1). This result indicates that the C-terminal half has a stimulatory effect on inverse RNA–DNA strand exchange. We then sought to determine whether the C-terminal fragment also has the ability to enhance the inverse DNA–DNA strand exchange reaction in *trans* (Supplementary Fig. S2A and B). When the inverse DNA–DNA strand exchange reaction was performed in the presence of RAD52-N, approximately 40% of dsDNA substrates were converted into products without RAD52-C (Fig. 4D and Supplementary Fig. S2C). In the presence of RAD52-C, a stimulatory effect was not observed (Fig. 4D and Supplementary Fig. S2C), as in the case of the inverse RNA–DNA strand exchange reaction. These results indicate that the stimulatory effect displayed by the C-terminal half is specific for the inverse RNA–DNA strand exchange reaction.

We further examined whether the stoichiometry of RAD52-N and RAD52-C affects the inverse RNA–DNA strand exchange efficiency (Fig. 5A). To do so, we performed inverse RNA–DNA strand exchange reactions in the presence of 0.02-fold, 0.1-fold, 0.2-fold, 0.5-fold, 2-fold or 4-fold concentrations of RAD52-C with respect to RAD52-N (Fig. 5B and Supplementary Fig. S3). We found that half the amount of RAD52-C relative to RAD52-N was still effective in stimulating the reaction (Fig. 5B, left graph, top row). However, RAD52-C did not stimulate the reaction at or below 0.2-fold concentrations (Fig. 5B, bottom row). Moreover, excess amounts of RAD52-C relative to RAD52-N did not result in significantly higher yields of the products (Fig. 5B, middle and right graphs, top row). Thus, the RNA–DNA strand exchange efficiently occurred at or near equimolar concentrations of RAD52-N and RAD52-C. These observations suggest that the N- and

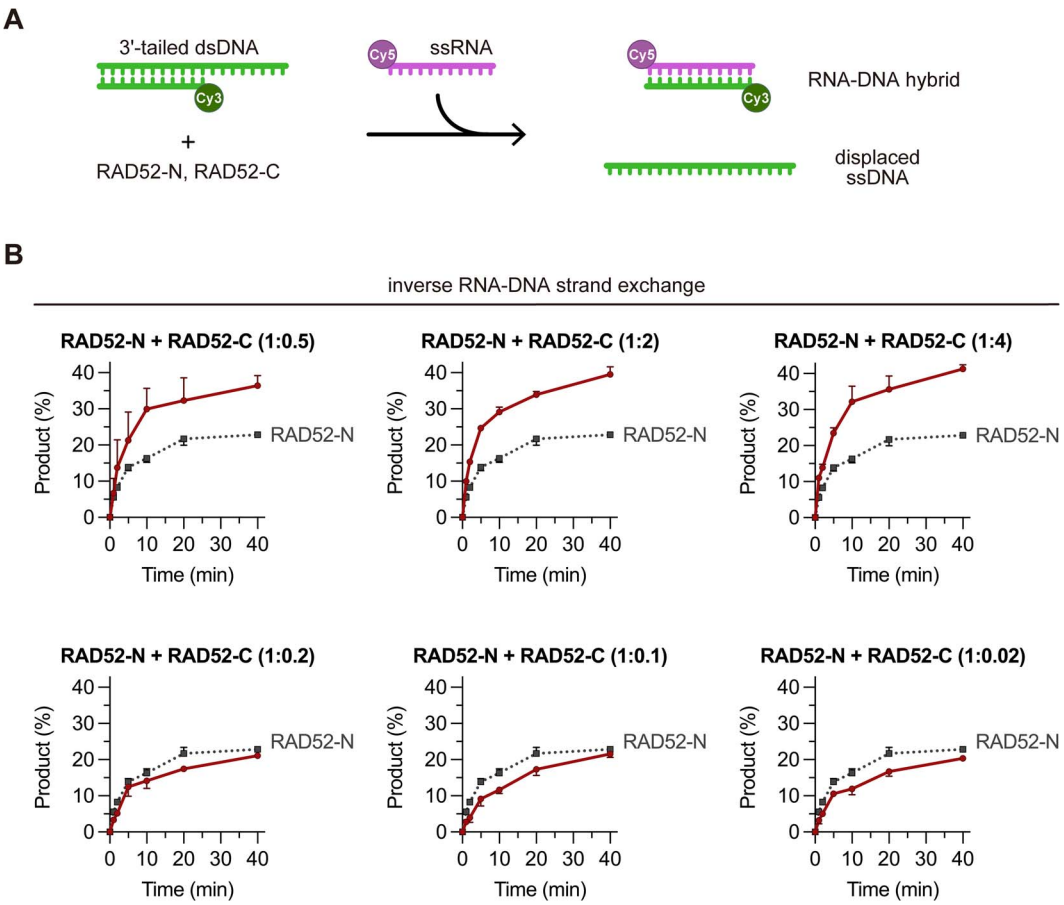


**Fig. 5. Effects of altering the molar ratio of the isolated N- and C-terminal domains of RAD52 in the inverse RNA–DNA strand exchange.** (**A**) A schematic diagram of the inverse RNA–DNA strand exchange reaction promoted by RAD52-N and RAD52-C. (**B**) Percentages of inverse RNA–DNA strand exchange catalysed in the presence of both RAD52-N and RAD52-C (shown in dark red). The molar ratios are shown in parentheses. In all assays, the final concentration of RAD52-N was 1 $\mu$M. All assays were repeated three times independently. Graphs show averages of three independent experiments. The error bars represent the standard deviation. To facilitate comparison, the inverse strand exchange activity of RAD52-N is shown as a dotted line in each graph.

C-terminal halves of RAD52 may interact with each other in a stoichiometric manner in the presence of ssRNA.

We also investigated whether the C-terminal half stimulates the forward RNA–DNA strand exchange reaction in *trans* (Fig. 6A). Consistent with previous reports *(12)*, the full-length RAD52 protein promoted the forward RNA–DNA strand exchange reaction, but with reduced efficiency (Fig. 6B and Supplementary Fig. S4). In contrast to the nearly 2-fold difference in product formation between the full-length protein and RAD52-N in the inverse RNA–DNA strand exchange, the forward strand exchange activities of the full-length protein and RAD52-N were nearly the same (Fig. 6B and Supplementary Fig. S4). The inclusion of RAD52-C did not stimulate the forward RNA–DNA strand exchange reaction that was promoted by RAD52-N (Fig. 6B and Supplementary Fig. S4). Thus, the stimulation of the RAD52-N driven strand exchange by RAD52-C in *trans* appears to occur only with the dsDNA and ssRNA combination in an inverse mechanism.

## Discussion

The present work further extends our knowledge of the interactions between RAD52 and ssRNA and provides clues as to how RAD52 may function in RNA-dependent DSB repair. RAD52 stably associated with ssRNA and ssDNA, with comparable affinities. From the domain analysis, we found that the primary binding site for ssRNA resides in the N-terminal half of RAD52. The isolated N-terminal half retained partial inverse RNA–DNA strand exchange activity. This region also has binding sites for ssDNA and is responsible for stimulating the annealing reaction between complementary DNA strands. Thus, it seems reasonable to conclude that the N-terminal half is also the catalytic site for promoting the formation of RNA–DNA hybrids.

Our finding that the isolated C-terminal half of RAD52 stimulates inverse RNA–DNA strand exchange, but not inverse DNA–DNA strand exchange, in *trans* suggests that the C-terminal half may play a key role in RNA-dependent DSB repair. To our knowledge, this is the first demonstration that the C-terminal half has functions other than binding RPA or RAD51 and providing sites for post-translational modifications. It is intriguing that equimolar concentrations of the isolated N- and C-terminal halves displayed similar RNA–DNA strand exchange activities as the full-length protein, despite the physical separation of these regions. A possible explanation for these results is that the N- and C-terminal halves associate with each other

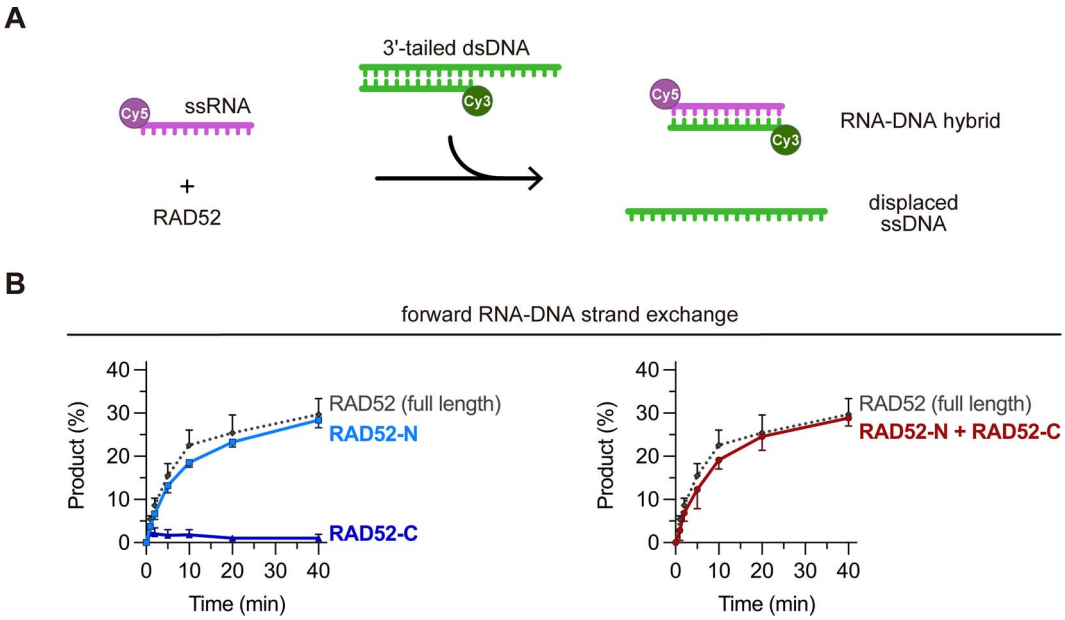


**Fig. 6. Forward RNA–DNA strand exchange activities of the isolated N- and C-terminal domains of RAD52.** (**A**) A schematic diagram of the forward RNA–DNA strand exchange reaction promoted by RAD52. (**B**) Percentages of forward RNA–DNA strand exchange catalysed by the full-length RAD52 protein (1 $\mu$M), RAD52-N (1 $\mu$M), RAD52-C (1 $\mu$M) and both RAD52-N (1 $\mu$M) and RAD52-C (1 $\mu$M), plotted as a function of time. All assays were repeated three times independently. Graphs show averages of three independent experiments. The error bars represent the standard deviation.

in a stoichiometric manner, in the presence of ssRNA. More work is required to verify this hypothesis.

We further demonstrated that the RAD52-N driven, forward RNA–DNA strand exchange was not stimulated by RAD52-C in *trans*. The forward RNA–DNA strand exchange activities of the full-length RAD52 protein and RAD52-N were nearly the same, and the C-terminal half appeared to be dispensable in this reaction. This is contrary to the observations of the inverse RNA–DNA strand exchange, where the absence of the C-terminal half results in a nearly 2-fold decrease in strand exchange efficiency. Hence, a mechanism in which dsDNA associates with the RAD52-ssRNA nucleoprotein complex by random collision can be envisaged. In the inverse RNA–DNA strand exchange promoted by RAD52, it is tempting to speculate that the C-terminal half of RAD52 recruits the ssRNA to the catalytic site in the N-terminal half where the dsDNA is bound. These observations further support the view that the trans-stimulation by RAD52-C is specific to the inverse RNA–DNA strand exchange.

Although the precise roles of the C-terminal half of RAD52 in RNA-dependent DSB repair remain to be elucidated, hints towards clarifying its functions may also be obtained from the structural properties of this region. For example, bioinformatic analyses of the human RAD52 protein predicted that the C-terminal half is mostly intrinsically disordered *(34, 35)*. Many RNA-binding proteins with intrinsically disordered regions have been implicated in phase separation *(45)*. Taken together with our finding that the C-terminal half physically interacts with ssRNA, this region may promote liquid–liquid phase separation. Previously, the yeast Rad52 protein was shown to form liquid-like droplets both *in vivo* and *in vitro (46)*. The droplet formation by Rad52 reportedly facilitates the assembly of DNA repair centers at the nuclear periphery. Thus, it is tempting to speculate that RAD52 may be involved in RNA-dependent DSB repair via liquid–liquid phase separation promoted by its C-terminal half.

## Data availability

All data are contained in the article or available from the corresponding author upon request.

## Funding

This work was supported in part by the Japan Society for the Promotion of Science, KAKENHI (19K12328, 20H00449 and 22H03743 to WK) and by the Priority Research Funding from Meisei University.

## Supplementary Data

Supplementary Data are available at *JB Online*.

## Conflict of interest

The authors declare that they have no conflicts of interest with the contents of this article.

## REFERENCES

1. Mehta, A. and Haber, J.E. (2014) Sources of DNA double-strand breaks and models of recombinational DNA repair. *Cold Spring Harb. Perspect. Biol.* **6**, a016428 1-17
2. Ceccaldi, R., Rondinelli, B., and D'Andrea, A.D. (2016) Repair pathway choices and consequences at the double-strand break. *Trends Cell Biol.* **26**, 52–64
3. Jackson, S.P. and Bartek, J. The DNA-damage response in human biology and disease. *Nature* **461**, 1071–1078
4. Ciccia, A. and Elledge, S.J. (2010) The DNA damage response: making it safe to play with knives. *Mol. Cell* **40**, 179–204

5. Daley, J.M., Gaines, W.A., Kwon, Y., and Sung, P. (2014) Regulation of DNA pairing in homologous recombination. *Cold Spring Harb. Perspect. Biol.* **6**, a017954 1-15
6. Marnef, A., Cohen, S., and Legube, G. (2017) Transcription-coupled DNA double-strand break repair: active genes need special care. *J. Mol. Biol.* **429**, 1277–1288
7. Bouwman, B.A.M. and Crosetto, N. (2018) Endogenous DNA double-strand breaks during DNA transactions: emerging insights and methods for genome-wide profiling. *Genes* **9**, 632
8. Yasuhara, T., Kato, R., Hagiwara, Y., Shiotani, B., Yamauchi, M., Nakada, S., Shibata, A., and Miyagawa, K. (2018) Human Rad52 promotes XPG-mediated R-loop processing to initiate transcription-associated homologous recombination repair. *Cell* **175**, 558–570.e11
9. Keskin, H., Shen, Y., Huang, F., Patel, M., Yang, T., Ashley, K., Mazin, A.V., and Storici, F. (2014) Transcript-RNA-templated DNA recombination and repair. *Nature* **515**, 436–439
10. Wei, L., Nakajima, S., Bohm, S., Bernstein, K.A., Shen, Z., Tsang, M., Levine, A.S., and Lan, L. (2015) DNA damage during the G0/G1 phase triggers RNA-templated, Cockayne syndrome B-dependent homologous recombination. *Proc. Natl. Acad. Sci. U. S. A.* **112**, E3495–E3504
11. Welty, S., Teng, Y., Liang, Z., Zhao, W., Sanders, L.H., Greenamyre, J.T., Rubio, M.E., Thathiah, A., Kodali, R., Wetzel, R., Levine, A.S., and Lan, L. (2018) RAD52 is required for RNA-templated recombination repair in post-mitotic neurons. *J. Biol. Chem.* **293**, 1353–1362
12. Mazina, O.M., Keskin, H., Hanamshet, K., Storici, F., and Mazin, A.V. (2017) Rad52 inverse strand exchange drives RNA-templated DNA double-strand break repair. *Mol. Cell* **67**, 1–11
13. Kasahara, M., Clikeman, J.A., Bates, D.B., and Kogoma, T. (2000) RecA protein-dependent R-loop formation in vitro. *Genes Dev.* **14**, 360–365
14. Zaitsev, E.N. and Kowalczykowski, S.C. (2000) A novel pairing process promoted by *Escherichia coli* RecA protein: inverse DNA and RNA strand exchange. *Genes Dev.* **14**, 740–749
15. McDevitt, S., Rusanov, T., Kent, T., Chandramouly, G., and Pomerantz, R.T. (2018) How RNA transcripts coordinate DNA recombination and repair. *Nat. Commun.* **9**, 1091
16. Mortensen, U.H., Bendixen, C., Sunjevaric, I., and Rothstein, R. (1996) DNA strand annealing is promoted by the yeast Rad52 protein. *Proc. Natl. Acad. Sci. U. S. A.* **93**, 10729–10734
17. Sugiyama, T., New, J.H., and Kowalczykowski, S.C. (1998) DNA annealing by RAD52 protein is stimulated by specific interaction with the complex of replication protein a and single-stranded DNA. *Proc. Natl. Acad. Sci. U. S. A.* **95**, 6049–6054
18. Reddy, G., Golub, E.I., and Radding, C.M. (1997) Human Rad52 protein promotes single-strand DNA annealing followed by branch migration. *Mutat. Res.* **377**, 53–59
19. Bhargava, R., Onyango, D.O., and Stark, J.M. (2016) Regulation of single-strand annealing and its role in genome maintenance. *Trends Genet.* **32**, 566–575
20. Ivanov, E.L., Sugawara, N., Fishman-Logell, J., and Haber, J.E. (1996) Genetic requirements for the single-strand annealing pathway of double-strand break repair in *Saccharomyces cerevisiae*. *Genetics* **142**, 693–704
21. Asleson, E.N., Okagaki, R.J., and Livingston, D.M. (1999) A core activity associated with the N terminus of the yeast *RAD52* protein is revealed by *RAD51* overexpression suppression of C-terminal *rad52* truncation alleles. *Genetics* **153**, 681–692
22. Kagawa, W., Kagawa, A., Saito, K., Ikawa, S., Shibata, T., Kurumizaka, H., and Yokoyama, S. (2008) Identification of a second DNA binding site in the human Rad52 protein. *J. Biol. Chem.* **283**, 24264–24273
23. Kagawa, W., Kurumizaka, H., Ikawa, S., Yokoyama, S., and Shibata, T. (2001) Homologous pairing promoted by the human Rad52 protein. *J. Biol. Chem.* **276**, 35201–35208
24. Hanamshet, K. and Mazin, A.V. (2020) The function of RAD52 N-terminal domain is essential for viability of BRCA-deficient cells. *Nucleic Acids Res.* **48**, 12778–12791
25. Shinohara, A., Shinohara, M., Ohta, T., Matsuda, S., and Ogawa, T. (1998) Rad52 forms ring structures and co-operates with RPA in single-strand DNA annealing. *Genes Cells* **3**, 145–156
26. Stasiak, A.Z., Larquet, E., Stasiak, A., Müller, S., Engel, A., Van Dyck, E., West, S.C., and Egelman, E.H. (2000) The human Rad52 protein exists as a heptameric ring. *Curr. Biol.* **10**, 337–340
27. Kinoshita, C., Takizawa, Y., Saotome, M., Ogino, S., Kurumizaka, H., and Kagawa, W. (2023) The cryo-EM structure of full-length RAD52 protein contains an undecameric ring. *FEBS Open Bio.* **13**, 408–418
28. Kagawa, W., Kurumizaka, H., Ishitani, R., Fukai, S., Nureki, O., Shibata, T., and Yokoyama, S. (2002) Crystal structure of the homologous-pairing domain from the human Rad52 recombinase in the undecameric form. *Mol. Cell* **10**, 359–371
29. Singleton, M.R., Wentzell, L.M., Liu, Y., West, S.C., and Wigley, D.B. (2002) Structure of the single-strand annealing domain of human RAD52 protein. *Proc. Natl. Acad. Sci. U. S. A.* **99**, 13492–13497
30. Saotome, M., Saito, K., Yasuda, T., Ohtomo, H., Sugiyama, S., Nishimura, Y., Kurumizaka, H., and Kagawa, W. (2018) Structural basis of homology-directed DNA repair mediated by RAD52. *iScience* **3**, 50–62
31. Lloyd, J.A., McGrew, D.A., and Knight, K.L. (2005) Identification of residues important for DNA binding in the full-length human Rad52 protein. *J. Mol. Biol.* **345**, 239–249
32. Rothenberg, E., Grimme, J.M., Spies, M., and Ha, T. (2008) Human Rad52-mediated homology search and annealing occurs by continuous interactions between overlapping nucleoprotein complexes. *Proc. Natl. Acad. Sci. U. S. A.* **105**, 20274–20279
33. Grimme, J.M., Honda, M., Wright, R., Okuno, Y., Rothenberg, E., Mazin, A.V., Ha, T., and Spies, M. (2010) Human Rad52 binds and wraps single-stranded DNA and mediates annealing via two hRad52-ssDNA complexes. *Nucleic Acids Res.* **38**, 2917–2930
34. Jumper, J., Evans, R., Pritzel, A., Green, T., Figurnov, M., Ronneberger, O., Tunyasuvunakool, K., Bates, R., Žídek, A., Potapenko, A., Bridgland, A., Meyer, C., Kohl, S.A.A., Ballard, A.J., Cowie, A., Romera-Paredes, B., Nikolov, S., Jain, R., Adler, J., Back, T., Petersen, S., Reiman, D., Clancy, E., Zielinski, M., Steinegger, M., Pacholska, M., Berghammer, T., Bodenstein, S., Silver, D., Vinyals, O., Senior, A.W., Kavukcuoglu, K., Kohli, P., and Hassabis, D. (2021) Highly accurate protein structure prediction with AlphaFold. *Nature* **596**, 583–589
35. Varadi, M., Anyango, S., Deshpande, M., Nair, S., Natassia, C., Yordanova, G., Yuan, D., Stroe, O., Wood, G., Laydon, A., Žídek, A., Green, T., Tunyasuvunakool, K., Petersen, S., Jumper, J., Clancy, E., Green, R., Vora, A., Lutfi, M., Figurnov, M., Cowie, A., Hobbs, N., Kohli, P., Kleywegt, G., Birney, E., Hassabis, D., and Velankar, S. (2022) AlphaFold protein structure database: massively expanding the structural coverage of protein-sequence space with high-accuracy models. *Nucleic Acids Res.* **50**, D439–D444
36. Plate, I., Hallwyl, S.C.L., Shi, I., Krejci, L., Müller, C., Albertsen, L., Sung, P., and Mortensen, U.H. (2008) Inter-

action with RPA is necessary for Rad52 repair center formation and for its mediator activity. *J. Biol. Chem.* **283**, 29077–29085
37. Park, M.S., Ludwig, D.L., Stigger, E., and Lee, S.-H. (1996) Physical interaction between human RAD52 and RPA is required for homologous recombination in mammalian cells. *J. Biol. Chem.* **271**, 18996–19000
38. Krejci, L., Song, B., Bussen, W., Rothstein, R., Mortensen, U.H., and Sung, P. (2002) Interaction with Rad51 is indispensable for recombination mediator function of Rad52. *J. Biol. Chem.* **277**, 40132–40141
39. Shen, Z., Cloud, K.G., Chen, D.J., and Park, M.S. (1996) Specific interactions between the human RAD51 and RAD52 proteins. *J. Biol. Chem.* **271**, 148–152
40. Song, B.W. and Sung, P. (2000) Functional interactions among yeast Rad51 recombinase, Rad52 mediator, and replication protein a in DNA strand exchange. *J. Biol. Chem.* **275**, 15895–15904
41. Sugiyama, T. and Kowalczykowski, S.C. (2002) Rad52 protein associates with replication protein a (RPA)-single-stranded DNA to accelerate Rad51-mediated displacement of RPA and presynaptic complex formation. *J. Biol. Chem.* **277**, 31663–31672
42. Seong, C., Sehorn, M.G., Plate, I., Shi, I., Song, B., Chi, P., Mortensen, U., Sung, P., and Krejci, L. (2008) Molecular anatomy of the recombination mediator function of *Saccharomyces cerevisiae* Rad52. *J. Biol. Chem.* **283**, 12166–12174
43. Green, M.R. and Sambrook, J. (2012) *Molecular Cloning. A Laboratory Manual*. pp130–132 Cold Spring Harbor Laboratory Press, Cold Spring Harbor, NY
44. Schindelin, J., Arganda-Carreras, I., Frise, E., Kaynig, V., Longair, M., Pietzsch, T., Preibisch, S., Rueden, C., Saalfeld, S., Schmid, B., Tinevez, J.-Y., White, D.J., Hartenstein, V., Eliceiri, K., Tomancak, P., and Cardona, A. (2012) Fiji: an open-source platform for biological-image analysis. *Nat. Methods* **9**, 676–682
45. André, A.A.M. and Spruijt, E. (2020) Liquid-liquid phase separation in crowded environments. *Int. J. Mol. Sci.* **21**, 5908
46. Oshidari, R., Huang, R., Medghalchi, M., Tse, E.Y.W., Ashgriz, N., Lee, H.O., Wyatt, H., and Mekhail, K. (2020) DNA repair by Rad52 liquid droplets. *Nat. Commun.* **11**, 695